Manuscript prepared for The Cryosphere
with version 4.2 of the LaTeX class copernicus.cls.
Date: 31 August 2014

Influence of stress, temperature and crystal morphology on isothermal densification and specific surface area decrease of new snow

S. Schleef, H. Löwe, and M. Schneebeli

WSL Institute for Snow and Avalanche Research SLF, Davos, Switzerland

Correspondence to: Henning Löwe
(loewe@slf.ch)

Abstract. Laboratory-based, experimental data for the microstructural evolution of new snow is scarce, though applications would benefit from a quantitative characterization of the main influences. To this end we have analyzed the metamorphism and concurrent densification of new snow under isothermal conditions by means of X-ray microtomography and compiled a comprehensive data set of 45 time series. In contrast to previous measurements on isothermal metamorphism on time scales of weeks to months, we analyzed the initial 24-48 h of snow evolution at high temporal resolution of three hours. The data set comprised natural and laboratory-grown snow and experimental conditions included systematic variations of overburden stress, temperature and crystal habit to address the main influences on specific surface area (SSA) decrease rate and densification rate in a snowpack. For all conditions we found a linear relation between density and SSA, indicating that metamorphism has an immediate influence for the densification of new snow. The slope of the linear relation however depends on the other parameters which were analyzed individually to derive a best-fit parametrization for the SSA decrease rate and the densification rate. In the investigated parameter range, we found that the initial value of the SSA constituted the main morphological influence on the SSA decrease rate. In turn, the SSA decrease rate constituted the main influence on the densification rate.

1 Introduction

The temporal evolution of new snow is delicate, since fast changes of bulk density or specific surface area (SSA) as key microstructural characteristics occur within hours after snowfall. Various applications rely on a quantitative understanding of these initial snowpack processes. For avalanche

prediction a fast or slowly densifying snowpack eventually discerns between conditions of high or low snowpack stability. Initial modeling uncertainties of the densification will propagate and persist through the entire season (Steinkogler et al., 2009). The density of snow is also important for hydrological applications where estimates of snow water equivalent are commonly obtained from snow height measurements of meteorological stations via empirical correlations between height and density. The development of these parametrizations is complicated by intermediate snow falls and short time densification (McCreight and Small, 2014). If the state of the snowpack is instead monitored via remote sensing, the key quantity is snow albedo which is mainly determined via SSA (Flanner and Zender, 2006). Even thin layers of new snow have a measurable impact on the total snow albedo (Perovich, 2007). Finally, the validation of winter precipitation schemes for meteorological models also relies on the connection between airborne crystal sizes (which might be related to the inverse SSA) and the bulk densities of new snow (Thompson et al., 2008).

For many applications ground-truth measurements are not available and the evolution of new snow on the ground must be addressed by snowpack modeling. Snowpack models primarily aim at a description of densification rates in terms of overburden and temperature (Jordan, 1991; Lehning et al., 2002; Vionnet et al., 2012). To cope with the needs of applications for metrics of crystal size and morphology, some of the models also include empirical, microstructural parameters such as grain size, dendricity, sphericity or coordination number. The choice of these microstructural parameters is motivated by the natural variation of snow crystal habits plus some metric of connectivity. These empirical parameters are however ambiguous and cannot be measured objectively for aggregated snow. Therefore recent versions of snowpack models have replaced the empirical parameters by objective ones which can be uniquely defined for arbitrary bicontinuous structures. Of primary interest was the replacement of grain size by the SSA (or more precisely, the optical radius) (Carmagnola et al., 2014) which is considered as the most important, morphological parameter of snow which can be measured in the field by various techniques.

Besides SSA, there is certainly a demand for higher-level morphological metrics to characterize snow microstructure. Various physical properties have been shown to be influenced by morphological characteristics beyond the SSA, e.g. thermal conductivity (Löwe et al., 2013) by anisotropy, the extinction of light (Libois et al., 2013) by grain shape, the scattering of microwaves by correlation lengths (Wiesmann et al., 1998) or confined compression of new snow by the Euler characteristic (Schleef et al., 2014b). The Euler characteristic is a topological metric for the connectivity of the structure (Michelsen et al., 2003). One one hand it might be regarded as a generalization of the grain-based concept of a coordination number (Lehning et al., 2002) to arbitrary 3D microstructures. On the other hand, the Euler characteristic is also exactly related to the average Gaussian curvature. The Euler characteristic thus constitutes a link to structure characterization in terms of full distributions of interfacial curvatures as a high-level morphological metric. This has e.g. been recently used to reveal details of temperature gradient metamorphism (Calonne et al., 2014). These recent advances

in microstructural insight are indeed necessary and important, but none of these higher-level morphological metrics have been implemented in snow models yet, not to mention the difficulties to measure them by methods other than micro-computed tomography (μCT). In the absence of advances to include or alternatively measure higher-level metrics, the density and the SSA must still be considered as the most important microstructural parameters for current snowpack models. A good representation of the time evolution of these parameters is a minimum requirement for these models. To reveal shortcomings of present models, there is a need to bridge from laboratory-based techniques (e.g. μCT) to field techniques to facilitate the validation of basic processes like metamorphism and densification under a wide range of environmental conditions.

From the perspective of laboratory experiments, some progress has been recently made to understand the physical mechanisms underlying new snow densification and metamorphism within creep experiments (Schleef and Löwe, 2013). The results indicate that the evolution of the SSA occurs autonomously without being affected by the concurrent densification. The experiments were carried out for a single type of snowmaker new snow (Schleef et al., 2014a) at a single temperature. However, this small range of experimental conditions is of only limited use for the aforementioned applications and the validation of models. To cover a wide range of environmental conditions for snow types and temperatures, applications are interested in best-fit behavior of large data sets which are essential benchmarks to validate and drive snow evolution models. From the perspective of field experiments, some data sets are available for well-aged seasonal snow (Dominé et al., 2007) and data of experiments which includes new snow in its first few days of evolution (Cabanes et al., 2002, 2003; Legagneux et al., 2003; Taillandier et al., 2007). But comparable data from in-situ experiments which monitor the evolution of the *same* sample of new snow at high temporal resolution is almost non-existent.

To fill this gap we present a comprehensive data set of μCT experiments for new snow densification and metamorphism covering various examples of natural and laboratory-grown new snow with a wide range of initial crystal morphologies. The primary goal of the present work is to provide laboratory-based experimental data for validation purposes. Our aim is to bridge from high-level laboratory experiments to the capabilities of field measurements by assessing, if densification and metamorphism under isothermal conditions can be described by the most important, yet available, parameters for snow models, namely the density, temperature, overburden stress and the SSA. We focus on the SSA as the most important morphological metric for snow microstructure. To relate to the original idea of crystal classification, we include a qualitative characterization of our experiments in terms of crystal habit classes. To make contact to recent high-level morphological metrics, we also analyze the Euler characteristic.

The outline of the paper is as follows. In section 2 we briefly summarize the methods for the experiments and the analysis which have been previously published elsewhere (Schleef and Löwe, 2013; Schleef et al., 2014a,b). We present in-situ creep experiments at different temperatures and

overburden stresses, and monitor the evolution of the main microstructural parameters, namely ice volume fraction ϕ_i and SSA over one to two days at a temporal resolution of 3 hours. A reference experiment over an entire week indicates that this is sufficient to capture the main aspects of microstructural changes. The results of the experiments are given in section 3. As an interesting generic result, we consistently find an almost linear relation between the density and the SSA, with different slopes, though, which depend on the specific conditions (section 3.2). In the following we separately discuss the influence of temperature (section 3.3) and morphological characteristics (section 3.4) on densification rate and SSA decrease rate. The different stress levels give rise to particularities which are pointed out. In section 3.5 we address the combined effects of all parameters on densification rate and SSA decrease rate. Based on our generic relation between SSA and density and based on previous modeling ideas we derive simple parametrizations for the rate equation of SSA and density for new snow in terms of the most important, yet available, parameters, namely ϕ_i, SSA, temperature T and stress σ. Our parametrization for the SSA is compared to an existing parametrization (Taillandier et al., 2007) in section 3.5. Finally, we discuss our results in section 4.

2 Methods

For a self-contained presentation we summarize the main steps of the method and outline differences or extensions to Schleef and Löwe (2013); Schleef et al. (2014a,b).

All snow samples were prepared from fresh snow, which was either collected outside or produced with a machine in the cold laboratory (Schleef et al., 2014a), referred to as natural snow and snowmaker snow, respectively. An overview of all sets of experiments with their main characteristics is given in Table 1. The natural snow was collected just outside the cold laboratory in Davos, Switzerland, during the winters 2011/2012 and 2012/2013. To minimize previous metamorphism, only intense snowfalls at air temperatures below -2°C with a deposition time less than an hour were chosen. Immediately afterwards the snow was sieved (mesh size 1 mm) into sample holders of 18 mm diameter with 15 mm filling height. In between, photographs of sieved snow crystals were taken to capture the crystal habit. Each set of snow samples comprised several identically prepared samples which were stored in a freezer at -60°C to nearly suppress metamorphism until the experiments (Kaempfer and Schneebeli, 2007). In total, 8 sets of snow samples from different natural snow falls and 6 sets from different snowmaker runs were prepared (Table 1). In Schleef and Löwe (2013) the potential bias caused by different storage times was addressed. We found that no systematic change of the SSA and density during storage times of three weeks at $-60°C$ in the SSA range of around 70 mm^{-1} could be measured by μCT. The storage influence observed for some samples (SSA: $\sim$2%, density: $\sim$5%) is generally small compared to the observed evolution during the experiments.

All experiments were conducted within at most 3 weeks after sample preparation. The respective sample was placed in the cold laboratory one hour before the first measurement for thermal equili-

bration. For some experiments (Table 1) a cylindrical weight, corresponding to a stress of 133, 215 or 318 Pa, respectively, was carefully put on the sample half an hour before starting the first measurement to analyze the influence of external stress. Stress values were chosen to mimic different potential burial depths of new snow inside the snowpack. The stress values correspond to burial depths of about 0-30 cm, given an average new snow density of 100 kg m^{-3}.

The measurements were conducted with a desktop computer tomograph (μCT 80, SCANCO medical) operated in a cold laboratory at isothermal temperatures of about -13 or -18°C. For a single set (no. 14, cf. Table 1) the temperature was varied systematically to higher values of about -3 and -8°C to investigate the influence of temperature. For these samples, the temperature was recorded during the whole experiment with a sensor (iButton device) in the sealing cap of the sample holder. All samples were kept undisturbed in the μCT during the whole experiment which took one or two days. In one case, the measurement was extended to an entire week. μCT scans of a fixed (cylindrical) sub-volume in the middle of the sample with total height of 6.3 mm were conducted automatically with a time-interval of 3 hours. The nominal resolution was 10 μm voxel size and the energy 45 kV. One scan took about two hours. In total, 45 time series were measured leading to more than 600 μCT scans.

For the analysis, a cubic volume of 6.3 mm edge length was extracted for each measurement and segmented into a binary file of ice and air. From the resulting 3D images the ice fraction and the specific surface area was calculated (details in Schleef and Löwe (2013)). In the following the results are exclusively presented in terms of the the ice volume fraction ϕ_i which is directly obtained from the μCT. The volume fraction can be related to the snow density via $\rho = \phi_\mathrm{i}\rho_\mathrm{i}$ with the temperature dependent density of ice $\rho_\mathrm{i} = 917 - 920\mathrm{kg\,m}^{-3}$ (0 to -20°C) (Petrenko and Whitworth, 1999). For the SSA we use the definition as surface area per ice volume, which is related to the surface area per ice mass (SSA$_m$) by SSA= ρ_i SSA$_m$.

Though we mainly focus on the ice volume fraction and the SSA for the analysis we have additionally evaluated the Euler characteristic χ of the samples. The Euler characteristic provides information about the topology which has been proven useful to understand the evolution of the snow microstructure under forced compression in a micro-compression device (Schleef et al., 2014b). The Euler characteristic $\chi = 2 - 2g$ is related to the interface genus g which is an indicator for the connectivity of a structure (cf. e.g. Michelsen et al. (2003)). The Euler characteristic typically assumes negative values, corresponding to high positive values of the interface genus. The higher the genus, the lower χ and the higher the number of inter-particle contacts. We calculated the Euler characteristic from the integral geometric approach of Minkowski functionals outlined by Michelsen et al. (2003). In accordance to the calculation of the SSA as a surface area per *ice volume* we normalized the Euler characteristic χ by the ice volume.

For the isothermal tomography measurements and their analysis we refer to Schleef and Löwe (2013) for an elaborate description of the experimental details.

3 Results

3.1 Overview

The natural new snow samples show large variations in the initial values of SSA and density. The snowmaker samples also varied in their initial characteristics and parameters due to different temperature settings of the machine (Schleef et al., 2014a). Overall, the initial ice volume fractions ranged from about 0.05 to 0.12, the initial SSA values were in the range 62-105 mm^{-1}, and the initial χ values were between $-2 \cdot 10^5 \mathrm{mm}^{-3}$ and $-12 \cdot 10^5 \mathrm{mm}^{-3}$. The averaged initial values of ϕ_i and SSA of each new snow type are listed in Table 1. The initial values had an influence on the settling, yielding a faster densification for a lower initial ϕ_i and a faster SSA decay for a higher initial SSA, but also variations of other parameters like temperature and stress led to a high variability.

As a starting point for our subsequent analysis we show the entire data for the temporal evolution of the ice volume fraction and the SSA for all samples in Figure 1 and Figure 2, respectively. Despite the variability, some trends are immediately visible, e.g. an influence of the initial SSA on the subsequent decay. However, other trends which may be expected (e.g. a clear ordering of the densification rates according to the applied stress) are clearly absent. A more detailed analysis of the individual influences is necessary.

For one randomly selected sample of natural snow at -13°C we extended the observation to a whole week. From the analysis we obtained the evolution of ϕ_i and SSA at high temporal resolution, as shown in Figure 3. For the given example, no external stress was applied, but the volume fraction ϕ_i increased by more than 40% from an initial value of about 0.11. At the same time the SSA decreased from 77 mm^{-1} to 45 mm^{-1}. A widely confirmed decay law for the SSA (Legagneux et al., 2004; Flanner and Zender, 2006; Kaempfer and Schneebeli, 2007; Schleef and Löwe, 2013) is given by

$$\mathrm{SSA}(t) = \mathrm{SSA}(0) \left(\frac{\tau}{t+\tau} \right)^{1/n} \tag{1}$$

with the parameters τ and n. A fit to the SSA data is shown in Figure 3 with the parameters $\tau = 27$ h and $n = 3.8$ ($R^2 > 0.99$).

For a visual demonstration of the microstructural evolution we combined sections of the 3D images (snow 5) to a time-lapse movie which is provided as supplementary material. The densification and coarsening is clearly visible in the movie and occurs in the absence of recognizable particle rearrangements and the creation of new inter-particle contacts.

3.2 General relation between density and SSA

Despite the common trends in the evolution of the SSA and the density, there is an apparent variability of individual curves shown in the previous section. However, the coupled evolution of both turns out to be governed by a generic feature. As suggested by Figure 3, the increase of the volume fraction

ϕ_i seems to "mirror" the SSA decay. If the ice volume fraction ϕ_i is plotted versus the SSA for all series (Fig. 4) an almost linear relation between both is consistently revealed irrespective of the experimental conditions. Except for one sample, which showed no densification at all, all other series of measurements can be fitted to the empirical linear relation $\phi_\mathrm{i} = a \cdot \mathrm{SSA} + b$ with coefficient of variation $R^2 > 0.94$. The fit parameters vary in the range $a = [-2 \cdot 10^{-3}, -0.2 \cdot 10^{-3}]$ and $b = [0.08, 0.26]$ depending on applied stresses, temperatures or crystal habits, however, not in an apparent, systematic way, as shown in Figure 4. We note that likewise a logarithmic law $\ln(\phi_\mathrm{i}) = a' \cdot \mathrm{SSA} + b'$ could be fitted to the data, with values $a' = [-2 \cdot 10^{-2}, -0.3 \cdot 10^{-2}]$ and $b' = [-2.5, -0.4]$ and $R^2 > 0.93$. This logarithmic dependence was suggested by Legagneux et al. (2002); Dominé et al. (2007). The difficulty of discerning a logarithmic from a linear relation is not surprising since $\ln(x) \approx -1 + x$ for values x close to one where both models seem to be equally valid. A detailed analysis of the experimental parameters on the SSA evolution and the densification will be carried out below.

3.3 Influence of temperature

To investigate the influence of different (isothermal) temperatures we measured the settling for one set of samples (snow 14 in Table 1) at three different laboratory temperatures. The temperature of the samples was recorded continuously during the experiments resulting in mean values of -3.1°C, -8.3°C and -13.4°C. Even though additional fans were mounted inside the μCT to minimize temperature fluctuations, the temperature changed during each scan by up to $\pm$0.5°C due to the heating of the X-ray tube. In addition, the defrosting cycles of the cold laboratory heat exchanger caused small changes of the temperature twice a day. In total, the temperature fluctuations were at maximum $\pm$0.6°C during one day, with the largest changes for the mean temperature of -3.1°C. For each temperature, we conducted one series without a weight on the sample and another one with a weight corresponding to a stress of 133 Pa and analyzed the density and the SSA.

3.3.1 Densification rate

The initial ice volume fractions of the samples were about 0.06-0.09. For the samples without applied stress almost no densification was observed within one day. Therefore a clear dependency on the temperature could not be obtained from the data of these samples. In contrast, the series with an applied stress of 133 Pa showed a significant, steady densification of 27%-48% per day which is clearly influenced by the temperature. The temperature influence of the densification of snow is often described by an Arrhenius law (Bader, 1960; Arnaud et al., 2000; Kirchner et al., 2001; Delmas, 2013)

$$\dot{\phi}_\mathrm{i}/\phi_\mathrm{i} = \nu \exp\left(-\frac{E}{k_B T_K}\right) \tag{2}$$

with a rate constant ν, an activation energy E, the Boltzmann constant k_B and the temperature T_K in Kelvin. From the differences of the ice volume fraction between successive time steps we obtain the experimental densification rates. Following the Arrhenius law, the mean densification rates per hour

for each series are plotted against the inverse temperature in Kelvin in Figure 5. The horizontal error bars result from the measured temperature fluctuations whereas the vertical errors bars indicate the maximum deviations from the mean values. By fitting the results to Eq. (2) we find the parameters $\nu = 4.8 \cdot 10^8 \mathrm{h}^{-1}$ and $E = 0.56 \mathrm{eV}$ ($R^2 = 0.49$) for the experiments with a stress of 133 Pa. The same fit for the experiments without stress yields $\nu = 2.8 \mathrm{h}^{-1}$ and $E = 0.16 \mathrm{eV}$ ($R^2 = 0.99$), however, there was only a marginal change of the density.

3.3.2 SSA decrease rate

The initial SSA of the samples ranged between 70-78 mm^{-1}. For all samples a steady decay of 12-31% in one day could be measured. Figure 6 shows the mean SSA decay per hour with error bars calculated in the same way as described for the ice fraction evolution. The SSA decay increased significantly with higher temperatures. At a temperature of about -13°C the decay was almost independent of the applied stress. In contrast, for higher temperatures the experiments with a stress of 133 Pa showed an accelerated rate of SSA decay. The temperature influence can be best described with an empirical linear relation $\dot{\mathrm{SSA}} = \alpha T + \beta$ with the parameters $\alpha = -0.02$ and $\beta = -0.62$ ($R^2 > 0.99$) for the experiments with stress $\sigma = 0$, and $\alpha = -0.04$, $\beta = -0.99$ ($R^2 = 0.99$) for $\sigma = 133$ Pa. This is valid if the temperature is given in °C and $\dot{\mathrm{SSA}}$ in units mm^{-1}h^{-1}. In Figure 6 the experiments at higher temperatures and $\sigma = 133$ Pa have a disproportionate error on the SSA rate, which is caused by a much higher SSA difference between the first two measurements of the time series. By neglecting the first measurement, the difference of the SSA rate at high temperatures between the experiments with and without applied stress would only be small. The particularity of the first time step is revealed by the Euler characteristic, which is analyzed below.

3.4 Influence of other morphological properties

3.4.1 Euler characteristic

A few selected examples for the evolution of the Euler characteristic χ during one day are shown in Figure 7. For most experiments, the Euler characteristic χ increases monotonically with a decreasing rate. In these cases the rate increased slightly with increasing temperature, but an influence of external stress was not observed. This is shown for one example (snow 9 in Figure 7). For some experiments, at higher temperatures, this monotonic behavior of the Euler characteristic disappears. The measurement without applied stress (snow 14, -3°C, 0 Pa) shows a monotonic increase, similar to the other experiments at lower temperatures, similar to the evolution of the one-week measurement (snow 5) and similar to the experiments from Schleef and Löwe (2013) (snow 9). However, if the stress is changed to 133 Pa (snow 14 at -3°C, 133 Pa) a different non-monotonic evolution of the Euler characteristic at the beginning of the experiment is observed. After this initial phase, the connectivity decreased again monotonically (i.e. increase of χ) similar to the evolution of the corresponding

experiment without applied stress. The rate was however slightly lower. Such a significant decrease of the Euler characteristic within the first 3 hours between the first and the second measurement has been observed only for a few measurements, predominantly at higher temperature. This decrease of the Euler characteristic corresponds to an increase of the number of inter-particle contacts, which contributes to the decrease of the SSA (Schleef et al., 2014b). These cases gave rise to the larger error in the SSA rate for higher temperatures in Figure 6.

3.4.2 Crystal habit

Finally we turn to apparent visual differences in the morphology of the crystals. From the photographs we compared the crystal habits of our samples to the classification of natural snow crystals (Kikuchi et al., 2013), as listed in Table 1. In most cases we observed broken parts of the respective crystal types, which might be caused by sieving. But also wind can lead to broken crystals in nature, and we could still identify the original crystal for the classification. An unambiguous classification for each snow sample was however not possible, because each sample contained a mixture of different habits. This was particularly the case for natural snow. For some samples, however, specific crystal habits dominated.

Figure 8 shows two examples of natural snow samples with a photo of the prominent crystal habit and the corresponding μCT image of the initial structure. The sample (Figure 8, bottom) is the one with the evolution shown in Figure 3 (snow 5 in Table 1), with dominant crystal habit of skeletal columns with scrolls (C3c) and combinations of columns and bullets (A1a). For comparison we picked another sample (Figure 8, top) which had almost the same initial ice fraction (snow 2 in Table 1) but a different dominating crystal habit (broad branches, P2b). This sample was unique since no densification at all could be measured within two days at -18°C, in contrast to the previous sample (snow 5) which showed a densification of about 18% within the same span at -13°C. However, the large difference cannot be explained by the temperature, because for all other samples there is no trend for the densification between the measurements at -13 or -18°C. There are also other samples with smaller differences in the densification rates for the same volume fraction and the same temperature and stress. In contrast, for the SSA decay rate no clear influence of the crystal habit has been found. In most cases the SSA evolution at the same temperature is identical for the same SSA values.

3.5 Combined influence of stress, temperature and morphology: Parametrizations

To provide an overall quantitative description of the SSA decrease rate and the densification rate which accounts for all measured quantities, we set up a parametrization based on our observations and existing concepts from literature.

3.5.1 SSA decrease rate

For the SSA decrease we start from the widely used power law given in Eq. (1). This is motivated by the very good agreement of Eq. (1) for the one-week measurement (Figure 3) even though also other functional forms are discussed in literature (Taillandier et al., 2007). To proceed, we note that Eq. (1) is the solution of the differential rate equation

$$\dot{\mathrm{SSA}} = A \cdot \mathrm{SSA}^m \tag{3}$$

if the parameters from Eq. (1) are chosen according to $n = m - 1$ and $\tau = -\frac{1}{An}\mathrm{SSA}(0)^{-n}$. The proportionality of τ to $\mathrm{SSA}(0)^{-n}$ is in accordance with the derivation from Legagneux et al. (2004). On the other hand our observations from section 3.3 indicate a linear influence of the temperature on the SSA decrease rate. But no influence on the applied stress has been observed during coarsening, except one case discussed in section 3.3.2. In addition, we have observed that for some cases the initial SSA rates are influenced by topological changes during densification (Fig. 7), as described by the Euler characteristic χ (section 3.4.1). In summary we chose the following form for the statistical model

$$\dot{\mathrm{SSA}} = (a + bT)\mathrm{SSA}^m + c\dot{\chi} \tag{4}$$

with the parameters a, b, c and m. Incorporating the topological influence $\dot{\chi}$ in an additive way in Eq. (4) is thereby in accordance to the relation found by compression experiments (Schleef et al., 2014b). Thereby, we consider that the SSA is not only affected by metamorphism but also by the number of contacts during settling between the ice grains. Crucial topological changes, i.e. the creation of new contacts within the structure, occurred only for a few samples at the beginning of the series of measurements.

A fit of Eq. (4) to the SSA rates obtained from the difference $\Delta\mathrm{SSA}/\Delta t$ of successive measurement within typically three hours for our complete data set yield $a = 2.9 \cdot 10^{-7}, b = 9.5 \cdot 10^{-9}, c = -3.5 \cdot 10^{-3}$ and $m = 3.5$ with $R^2 = 0.83$ (T in °C, SSA in mm^{-1} and $\dot{\chi}$ in mm^{-3}). The scatter plot between modeled and measured SSA rates is shown in Figure 9.

If we neglect the measurements where noticeable topological changes ($\dot{\chi} < 0$) occurred, which was only the case for ten samples for the first measurements, we could simplify the model to

$$\dot{\mathrm{SSA}} = (a' + b'T)\mathrm{SSA}^{m'}, \tag{5}$$

leading to fit parameters $a' = 1.1 \cdot 10^{-6}, b' = 3.1 \cdot 10^{-8}$ and $m' = 3.1$. In this case we obtain an even improved performance (R^2=0.87). This is particularly interesting, given the practical impossibility to measure the Euler characteristic without tomography.

3.5.2 Densification rate

A parametrization for the densification rate $\dot{\phi}_\mathrm{i}$ for all measurements turns out to be more complicated than for $\dot{\mathrm{SSA}}$, since $\dot{\phi}_\mathrm{i}$ is not only influenced by temperature and the initial value $\phi_{\mathrm{i},0}$ but also by the

stress and the crystal habit, as described before.

To motivate a model which aims to fit the entire data we start from the common stress dependence of the strain rate for visco-plastic flow of polycrystalline ice which is commonly described by Glen's law for secondary creep, $\dot{\varepsilon} = A\sigma^k$ (Petrenko and Whitworth, 1999). A similar form is believed to be valid for snow (Kirchner et al., 2001). In a one-dimensional system, the strain rate $\dot{\varepsilon}$ can be taken as the relative densification rate $\dot{\varepsilon} = \dot{\phi}_\mathrm{i}/\phi_\mathrm{i}$ (cf. also Schleef and Löwe (2013)) leading to

$$\dot{\phi}_\mathrm{i}/\phi_\mathrm{i} = A\sigma^k \tag{6}$$

with a constant A containing the rate of the process.

On the other hand we have empirically observed that the volume fraction is almost linearly related to the SSA (section 3.2). Hence we chose the rate in Eq. (6) to be determined mainly by the SSA rate, $A = B\,\dot{\mathrm{SSA}}$, and end up with

$$\dot{\phi}_\mathrm{i}/\phi_\mathrm{i} = B\,\dot{\mathrm{SSA}}\sigma^k \tag{7}$$

for our parametrization model, which includes two parameters, B and k. We note that integrating Eq. (7) in fact implies $\ln(\phi_\mathrm{i}) \sim \mathrm{SSA}$ and not a linear dependence. This is however in accordance with the result from section 3.2, where the logarithmic or the linear relation are indistinguishable. Thus Eq. (7) constitutes a reasonable trade off and naturally includes a dependence of the densification rate on the density itself.

A fit of Eq. (7) to the densification rates $\Delta\phi_\mathrm{i}/\Delta t$ obtained from successive measurements within typically three hours for our complete data set yields $B = -6.6 \cdot 10^{-3}$ and $k = 0.18$ (σ in Pa and $\dot{\mathrm{SSA}}$ in $\mathrm{mm^{-1}h^{-1}}$). We note that samples without a weight are assigned a remaining, non-zero stress of 5 Pa caused by the small but non-negligible overburden of the overlying snow inside the μCT sample holder on top of the evaluation cube. The same value was chosen by Schleef and Löwe (2013). The scatter plot between modeled and measured densification rates is shown in Figure 10, yielding $R^2 = 0.82$.

As suggested by the results from Schleef et al. (2014b), the Euler characteristic has an influence on the densification by discerning different connectivities. Accordingly, a slight improvement of the parametrization (7) is obtained by including the Euler characteristic via

$$\dot{\phi}_\mathrm{i}/\phi_\mathrm{i} = (B'\sigma^k + C'\dot{\chi})\dot{\mathrm{SSA}} \tag{8}$$

which yields $R^2 = 0.85$. In contrast to Eq. (4), where the additive dependence of the SSA decrease on the Euler characteristic was motivated by process insight (Schleef et al., 2014b), the inclusion of χ in (8) is purely empirical.

3.6 Comparison to an existing parametrization

Finally we compare our parametrization (5) for the SSA evolution to an existing parametrization from Taillandier et al. (2007), who derived a parametrization $\mathrm{SSA}_{\mathrm{T2007}}(t, T, \mathrm{SSA}(0))$ (Eq. (13) in

their paper) for the isothermal and quasi-isothermal evolution of the SSA with time t for given temperature T and initial value $\mathrm{SSA}(0)$. The parametrization was derived from SSA measurements which were conducted by the Brunauer–Emmett–Teller (BET) method of gas adsorption, with new snow samples collected after snowfall. With respect to the involved parameters, this is exactly equivalent to our parametrization $\mathrm{SSA}_{\mathrm{S2014}}(t,T,\mathrm{SSA}(0))$ which is obtained from integrating Eq. (5). To compare the overall trends of both parametrizations, we have computed the SSA difference after 48h, viz. $\Delta\mathrm{SSA}_X(48h) = \mathrm{SSA}_X(48\mathrm{h},T,\mathrm{SSA}(0)) - \mathrm{SSA}_X(0\mathrm{h},T,\mathrm{SSA}(0))$ for both formulations $X =$T2007,S2014, as a measure of the averaged SSA decay rate on the first day after snowfall. To use realistic values for $(T,\mathrm{SSA}(0))$ from real data-sets, we have evaluated the difference $\Delta\mathrm{SSA}_X(48h)$ for the present data set (45 tuples of $(T,\mathrm{SSA}(0))$), the isothermal experiments 1-9 from Taillandier et al. (2007) (9 tuples), and the experiments 1-5 from Legagneux et al. (2003) (5 tuples). The results are shown in Figure 11. A clear deviation from the 1:1 line is observed. In general our parametrization of the SSA decay rate is biased low compared to Taillandier et al. (2007). This bias remains, also if $\Delta\mathrm{SSA}_X(t)$ is evaluated for other times t. However, the parametrization T2007, based on BET measurements, and the parametrization S2014, based on μCT measurements, are clearly correlated. In both cases, the major influence on the SSA decrease rate stems from the initial value SSA(0).

4 Discussion

4.1 Main result

We start the discussion with the parametrization of the SSA and the densification for new snow under isothermal conditions (section 3.5). The parametrizations are motivated by available models for the SSA (Legagneux et al., 2004) and Glen's law for creep of polycrystalline ice (Petrenko and Whitworth, 1999). Conceptually, current snowpack models (Vionnet et al., 2012; Jordan, 1991; Bartelt and Lehning, 2002) use a similar approach for the densification, but still based on traditional grain size to characterize the microstructure. Only recently, the model Crocus was re-formulated (Carmagnola et al., 2014) to use SSA as the simplest, objective, morphological metric directly.

Our experiments focused only on new snow with low density and high SSA and most of our results are probably not valid for denser snow. In contrast to denser snow under isothermal metamorphism, we found that the densification rate is directly related to metamorphism via the SSA decrease rate. This is reflected by the consistent linear variation of the ice volume fraction with the SSA (Fig. 4). This observation was implemented in the parametrization by a prefactor in the densification rate which is proportional to the SSA rate. We have set up the parametrization for the densification in a way to guarantee that both evolution laws are only dependent on the quantities ϕ_{i} (or the density), the stress σ, the specific surface area SSA and the temperature T to best-fit the entire, available data of new snow. These quantities are directly available in snowpack models and Eqs. (5,7) provide

a closed set of empirical, microstructural evolution equations for the density and the SSA under isothermal conditions. Both microstructural parameters, SSA and density can be obtained in the field also without the use of tomography (Matzl and Schneebeli, 2006; Gallet et al., 2009; Arnaud et al., 2011).

4.2 Comparison to an existing parametrization

Our comparison with the parametrization from Taillandier et al. (2007) (section 3.6) has revealed that our parametrization (4) always underestimates the average SSA decay in 48h for given temperature and initial SSA when compared to their result (Figure 11). Different explanations for these deviations are possible. First, both parametrizations are based on different time scales. Our measurements focus only on the evolution of the SSA within typically two days, at high temporal resolution of 3h. In contrast, Taillandier et al. (2007) focuses on the evolution of the SSA over seasonal time scales from 1 to 100 days. Since their first measurement was conducted not before 24 hours, the parametrization in Taillandier et al. (2007) might lack accuracy in this initial stage. Thus for practical purposes a combination of both parametrizations might be envisaged to cover all time periods. Second, differences in the magnitude of temperature fluctuations might have an influence. If the isothermal experiments from Taillandier et al. (2007) were subject to temperature fluctuations larger than our accuracy of $\pm$0.6°C, these fluctuations might cause an increase of the SSA decay rate according to mechanisms mentioned in Pinzer and Schneebeli (2009). A quantitative estimate of this effect is however not yet possible. Third, a systematic error of the μCT measurements compared to BET measurements used in Taillandier et al. (2007) at these very high SSA values could not be ruled out. The comparison of BET and μCT from Kerbrat et al. (2008) has not revealed a systematic bias, though, but the uncertainty between both methods clearly increases at high SSA values. For very high SSA values, our μCT measurements with voxel size of 10μm are at the limit of the resolution. Ideally, remaining uncertainties about absolute values of very high SSA should be further investigated within dedicated inter-comparison experiments.

The origin of the remaining differences between both parametrizations could not be convincingly explained. However, the trends from Figure 11 obtained from the two parametrizations, which were based on different experimental techniques (μCT vs BET), are highly consistent. This motivates to measure the SSA of new snow also by other, less demanding techniques in the field. This will help to explore the influence of the initial SSA on new snow densification and improve the performance of snowpack models. Below we discuss the particularities of the SSA decrease rate and densification rate in view of the involved parameters.

4.3 SSA decrease rate

Our simple parametrization for the SSA change (4) yielded good agreement for almost all of our measurement data. The exponent m obtained from the fit must be compared to n from the widely

used Eq. (1) via $n = m - 1$, yielding $n = 2.5$. As already outlined by Schleef and Löwe (2013), the precise value of n is difficult to estimate, if the duration of the experiment is similar to τ, which is typically in the order of one day. This is confirmed by the one-week measurement which allowed a better estimate of the fit parameters in Eq. (1). The obtained exponent $n = 3.8$ agreed well with the results of Legagneux et al. (2004) who found $n = 3.4 - 5.0$ at a temperature of -15°C. In contrast, the results of the short time measurements did not lead to a conclusive estimate for n. Also the fits to the 2 day time series by Schleef and Löwe (2013) gave higher values of n and only an adapted combination of all series resulted in a similar n of about 3.9. However the value $n = 2.5$ indicates that, even for short times, the SSA decrease rate is dominantly influenced by the present value of the SSA in a non-linear way. It is generally believed that the value of n is also influenced by temperature, potentially caused by different underlying mechanisms of mass transport (Vetter et al., 2010; Löwe et al., 2011). In view of the difficulties of estimating n for the short time series, we have restricted ourselves to an inclusion of the temperature dependence into the prefactor in Eq. (4) to account for the acceleration of metamorphism at higher temperatures (Fig. 6).

We have previously observed that the SSA evolution was in fact independent of the densification or the applied stress, respectively (Schleef and Löwe, 2013). This was confirmed here for all experiments conducted at lower temperatures of -13°C or -18°C (cf Table 1). This behavior seems to be generally valid for all examined types of new snow. In addition, no difference could be observed between the evolution of sieved, natural new snow and snowmaker snow, which is in agreement to the results presented by Schleef et al. (2014a). The reason for the negligible stress dependence at low temperatures is that coarsening is the only relevant process. In these cases the Euler characteristic is a monotonic function with time (this is further explained below). At higher temperatures we have also observed cases where the Euler characteristic initially decreased. This is a clear indicator of structural re-arrangements and newly formed ice-ice contacts which contribute to the SSA decrease (Schleef et al., 2014b). This was however observed only for a few cases. If present, the structural re-arrangements and their impact on the SSA do depend on stress. This was revealed by the two (out of 584) $\Delta\mathrm{SSA}/\Delta t$ outliers in Figure 9. These are the first values of the series of measurements with an applied stress of 133 Pa at temperatures of -3°C and -8°C. Exactly for these measurement a significant, direct influence of the applied stress on the SSA evolution was observed which is not captured by the model (4). The data is however too limited to investigate this effect in greater detail. Apart from that, the parametrization Eq. (4), which is solely based on common snowpack model parameters, is well suited for modeling the SSA decrease of new snow.

4.4 Densification rate

The analysis of $\dot{\phi}_\mathrm{i}$ is based on the observation of the almost linear relation between the evolution of ϕ_i and SSA for each series of measurement (Fig. 4). Measurements of Legagneux et al. (2002); Dominé et al. (2007) show a logarithmic relation between density and SSA, which is however derived from

independent measurements in a seasonal snowpack and covers much wider SSA and density ranges. As outlined in section 3.2, a logarithmic relation for each of our series of measurement would also be possible here, and the linear relation might only be an approximation for short observation times. It is however not the functional form which is worth mentioning, it is rather the fact that the density evolution and the SSA evolution are intimately related.

In contrast to the SSA rate, a direct temperature dependence of the densification rate is less pronounced in the overall behavior. This stems from the fact that the main impact of densification comes from metamorphism itself via the SSA rate in Eq. (7), which implicitly contains a temperature dependence as discussed in the previous section. In general, one may expect also an explicit temperature dependence for the creep rate A in Eq. (7). The Arrhenius analysis of the temperature dependence for one of the sets for two stress values (Fig. 5) revealed that the densification is almost negligible for the case without weight. For the experiments with applied stress a faster rate of $\dot{\phi}_i/\phi_i$ could only be observed at about -3°C. The Arrhenius fit (2) yields an activation energy in the same order of magnitude as known for different possible processes in ice (about 1 eV, cf. Kirchner et al. (2001) and references therein), but the limited amount of data with just one series of measurement at -3°C and 133 Pa did not allow for conclusive parameter estimates. Obtaining reliable data for higher temperatures by desktop tomography is generally difficult, since the time scales for the fast structural changes of new snow are already in the order of the scanning times; image artifacts arise. Due to this technical limitation, most experiments were conducted at -13°C or -18°C where no general trend for a faster densification at higher temperatures could be observed.

4.5 The influence of other morphological parameters

Besides the most important microstructural parameters, density and SSA, we have also classified crystal habits to make contact to traditional characterization of crystal morphology and calculated the Euler characteristic, to make contact to more advanced morphological metrics.

4.5.1 Crystal habit

For selected examples, the classification of crystal habits has helped to empirically interpret experimental scatter. The examples in Figure 8 have shown that densification can easily differ by about 18%, which can not be explained by the temperature difference alone. Differences in crystal habit and their influence on the densification rate are not captured by our parametrization, which contains the SSA as the only morphological parameter. It seems unlikely that SSA is a sufficient morphological description of new snow type in the densification rate, as suggested by Eq. (7). However, for most of our measurements, the parametrization Eq. (7) works reasonably well, even though only two fit parameters are involved. In contrast, for the SSA evolution the crystal habit does not have an evident influence. Similar decay rates were found for samples with similar initial SSA but different crystal habits. Overall, the classification in terms of crystal habits was only of limited use. Some in-

fluence of the habit might be acknowledged, but future effort should rather aim at other quantitative, morphological parameters to explain the remaining scatter.

4.5.2 Euler characteristic

As suggested by recent compression experiments of new snow (Schleef et al., 2014b), the Euler characteristic might be a candidate morphological parameter to better interpret the evolution of SSA and density. Quantitatively, we have seen that the inclusion of the Euler characteristic in the parametrizations with Eqs. (4) and (8) only makes a slight difference for the very initial stage where some particle re-arrangements are noticeable. For the majority of samples we observed a monotonic increase of the Euler characteristic, or equivalently a monotonic decrease of the number of contacts. This is expected as a consequence of coarsening of bicontinuous morphologies alone (Kwon et al., 2007), where contacts, made of fine filaments, disappear. For a highly porous material like new snow, the slow creep deformation considered here does not cause significant structural re-arrangements and new contacts. This is confirmed also by visual inspection of the deformation in the movie (cf. supplementary material). For a few experiments, the Euler characteristic signaled an increase of the connectivity at the beginning. This was the case for samples with faster creep rates due to higher temperature, higher stresses or a very tenuous structures. In these cases, an influence on the evolution of SSA and ϕ_i can be observed, which is not captured by Eqs. (4) and (8). However, initial structural re-arrangements stabilize quickly. This is consistent with externally forced re-arrangements in deformation controlled compression experiments (Schleef et al., 2014b), in a less pronounced way, though.

Overall, the inclusion of the Euler characteristic as additional morphological parameter does not seem to be crucial for isothermal densification and metamorphism of new snow, at least for lower temperatures. However, the Euler characteristic has clearly helped to identify situations where the evolution was not only governed by coarsening alone. In common snowpack models, additional morphological information beyond SSA is empirically included in the dendricity parameter (Vionnet et al., 2012; Lehning et al., 2002). This parameter is actually not sufficiently exploited yet since new snow is always assigned the same dendricity, irrespective of the actual morphology of the crystals. The inclusion of an additional, objective parameter seems crucial, if the remaining scatter in SSA decrease rate and densification rate is an issue. To improve the understanding of new snow densification beyond Eq. (7) it seems important to replace also the dendricity by an objective microstructural parameter which captures relevant differences in crystal morphology. A candidate might be the anisotropy parameter Q as pursued by Löwe et al. (2013); Calonne et al. (2014) to reduce the scatter in the data for the thermal conductivity. A direct application of the methods from Löwe et al. (2013) is however not possible, since the correlation function for new snow can certainly not be approximated by a simple exponential form. A potential generalization of the methods from Löwe et al. (2013), tailored to the evolution of new snow, will be addressed in future work.

5 Conclusions

We have compiled a large data set of 45 time series (and a total of 600 μCT measurements) of in-situ experiments of new snow densification and metamorphism by μCT. For a quantitative characterization of all experiments, we have derived a parametrization for the SSA decrease and densification rate which performs reasonably well ($R^2 = 0.87, 0.82$, respectively) for the entire data set of of new snow experiments which were evaluated for the present analysis. The parametrization is only based on the parameters SSA, density, temperature, and stress, which are already available in current snowpack models, and which can be easily measured in the field. With these parameters, the main influences of metamorphism and densification of new snow can be quantitatively described. Advanced morphological metrics like the Euler characteristic give additional insight in the interpretation of the SSA and density evolution, the parametrizations have however not improved significantly upon inclusion of this parameter. This might be different for high temperatures, close to 0°C, where only few data is available due to the experimental limitations of μCT imaging for fast microstructural changes. It is however likely that an additional morphological parameter besides the SSA is required to reduce the remaining scatter in the description of new snow densification. This will require additional, theoretical work to guide the choice of a relevant parameter and suggest functional forms for parametrizations which improve existing ones.

The comparison of our parametrization for the SSA (as a function of time, temperature and initial SSA) with a formally equivalent one from Taillandier et al. (2007) has revealed a bias in the absolute values of SSA decrease, the trends of both formulations are however highly consistent. These trends can be probably also reproduced by simpler SSA retrieval methods (other than μCT or BET) which are more convenient to use in the field. This is important for further validation of snowpack models. We have shown that the rate of SSA decrease and thereby the SSA itself has probably the most dominant influence on isothermal densification of new snow. Hence, monitoring the SSA for operational purposes might greatly help to constrain the initial densification of snow after snowfall.

Acknowledgements. We thank Florent Dominé and two anonymous reviewers for their helpful suggestions on the manuscript. This work was funded by the Swiss National Science Foundation (SNSF) through Grant No. 200021 132549.

References

Arnaud, L., Barnola, J. M., and Duval, P.: Physical modeling of the densification of snow / firn and ice upper part of polar ice sheets, in: Physics of Ice Core Records, edited by Hondoh, T., vol. 159, pp. 285–305, Hokkaido University Press, Sapporo, Japan, 2000.

Arnaud, L., Picard, G., Champollion, N., Dominé, F., Gallet, J., Lefebvre, E., Fily, M., and Barnola, J.: Measurement of vertical profiles of snow specific surface area with a 1 cm resolution using infrared reflectance: instrument description and validation, J. Glaciol., 57, 17–29, 2011.

Bader, H.: Theory of densification of dry snow on high polar glaciers, US Army SIPRE Res. Rep., 69, 1960.

Bartelt, P. and Lehning, M.: A physical SNOWPACK model for the Swiss avalanche warning Part I: numerical model, Cold Reg. Sci. Technol., 35, 123–145, 2002.

Cabanes, A., Legagneux, L., and Dominé, F.: Evolution of the specific surface area and of crystal morphology of Arctic fresh snow during the ALERT 2000 campaign, Atmos. Environ., 36, 2767–2777, 2002.

Cabanes, A., Legagneux, L., and Dominé, F.: Rate of evolution of the specific surface area of surface snow layers, Environ. Sci. Technol., 37, 661–666, 2003.

Calonne, N., Flin, F., Geindreau, C., Lesaffre, B., and Rolland du Roscoat, S.: Study of a temperature gradient metamorphism of snow from 3-D images: time evolution of microstructures, physical properties and their associated anisotropy, Cryosphere Discuss., 8, 1407–1451, 2014.

Carmagnola, C. M., Morin, S., Lafaysse, M., Dominé, F., Lesaffre, B., Lejeune, Y., Picard, G., and Arnaud, L.: Implementation and evaluation of prognostic representations of the optical diameter of snow in the SURFEX/ISBA-Crocus detailed snowpack model, The Cryosphere, 8, 417–437, 2014.

Delmas, L.: Influence of snow type and temperature on snow viscosity, J. Glaciol., 59, 87–92, 2013.

Dominé, F., Taillandier, A.-S., and Simpson, W. R.: A parameterization of the specific surface area of seasonal snow for field use and for models of snowpack evolution, J. Geophys. Res., 112, 2007.

Flanner, M. G. and Zender, C. S.: Linking snowpack microphysics and albedo evolution, J. Geophys. Res., 111, 2006.

Gallet, J.-C., Dominé, F., Zender, C. S., and Picard, G.: Measurement of the specific surface area of snow using infrared reflectance in an integrating sphere at 1310 and 1550 nm, The Cryosphere, 3, 167–182, 2009.

Jordan, R.: A one-dimensional temperature model for a snow cover: Technical documentation for SNTHERM.89, CRREL Spec. Rep., 91-16, 1991.

Kaempfer, T. and Schneebeli, M.: Observation of isothermal metamorphism of new snow and interpretation as a sintering process, J. Geophys. Res., 112, 2007.

Kerbrat, M., Pinzer, B., Huthwelker, T., Gaeggeler, H., Ammann, M., and Schneebeli, M.: Measuring the specific surface area of snow with X-ray tomography and gas adsorption: comparison and implications for surface smoothness, Atmos. Chem. Phys., 8, 1261–1275, 2008.

Kikuchi, K., Kameda, T., Higuchi, K., and Yamashita, A.: A global classification of snow crystals, ice crystals, and solid precipitation based on observations from middle latitudes to polar regions, Atmos. Res., 132-133, 460–472, 2013.

Kirchner, H. O. K., Michot, G., Narita, H., and Suzuki, T.: Snow as a foam of ice: plasticity, fracture and the brittle-to-ductile transition, Philos. Mag. A, 81, 2161–2181, 2001.

Kwon, Y., Thornton, K., and Voorhees, P.: Coarsening of bicontinuous structures via nonconserved and con-

served dynamics, Phys. Rev. E, 75, 021 120, 2007.

Legagneux, L., Cabanes, A., and Dominé, F.: Measurement of the specific surface area of 176 snow samples using methane adsorption at 77 K, J. Geophys. Res., 107, 15, 2002.

Legagneux, L., Lauzier, T., Dominé, F., Kuhs, W., Heinrichs, T., and Techmer, K.: Rate of decay of specific surface area of snow during isothermal experiments and morphological changes studied by scanning electron microscopy, Can. J. Phys., 81, 459–468, 2003.

Legagneux, L., Taillandier, A.-S., and Dominé, F.: Grain growth theories and the isothermal evolution of the specific surface area of snow, J. Appl. Phys., 95, 6175, 2004.

Lehning, M., Bartelt, P., Brown, B., Fierz, C., and Satyawali, P.: A physical SNOWPACK model for the Swiss avalanche warning Part II. Snow microstructure, Cold Reg. Sci. Technol., 35, 147–167, 2002.

Libois, Q., Picard, G., France, J. L., Arnaud, L., Dumont, M., Carmagnola, C. M., and King, M. D.: Influence of grain shape on light penetration in snow, The Cryosphere, 7, 1803–1818, 2013.

Löwe, H., Spiegel, J., and Schneebeli, M.: Interfacial and structural relaxations of snow under isothermal conditions, J. Glaciol., 57, 499–510, 2011.

Löwe, H., Riche, F., and Schneebeli, M.: A general treatment of snow microstructure exemplified by an improved relation for thermal conductivity, Cryosphere, 7, 1473–1480, 2013.

Matzl, M. and Schneebeli, M.: Measuring specific surface area of snow by near-infrared photography, J. Glaciol., 52, 558–564, 2006.

McCreight, J. L. and Small, E. E.: Modeling bulk density and snow water equivalent using daily snow depth observations, The Cryosphere, 8, 521–536, 2014.

Michelsen, K., DeRaedt, H., and DeHosson, J.: Aspects of mathematical morphology, Adv. Imag. Elect. Phys., 125, 119–194, 2003.

Perovich, D. K.: Light reflection and transmission by a temperate snow cover, J. Glaciol., 53, 201–210, 2007.

Petrenko, V. F. and Whitworth, R. W.: Physics of ice, Oxford University Press, USA, 1999.

Pinzer, B. R. and Schneebeli, M.: Snow metamorphism under alternating temperature gradients: Morphology and recrystallization in surface snow, Geophys. Res. Lett., 36, L23 503, 2009.

Schleef, S. and Löwe, H.: X-ray microtomography analysis of isothermal densification of new snow under external mechanical stress, J. Glaciol., 59, 233–243, 2013.

Schleef, S., Jaggi, M., Löwe, H., and Schneebeli, M.: An improved machine to produce nature-identical snow in the laboratory, J. Glaciol., 60, 94–102, 2014a.

Schleef, S., Löwe, H., and Schneebeli, M.: Hot pressure sintering of low density snow analyzed by X-ray microtomography and in-situ micro-compression, Acta Mater., 71, 185–194, 2014b.

Steinkogler, W., Fierz, C., Lehning, M., and Obleitner, F.: Systematic Assessment of New Snow Settlement in SNOWPACK, in: International Snow Science Workshop, Davos, Switzerland, edited by Schweizer, J and VanHerwijnen, A, pp. 132–135, 2009.

Taillandier, A.-S., Dominé, F., Simpson, W. R., Sturm, M., and Douglas, T. a.: Rate of decrease of the specific surface area of dry snow: Isothermal and temperature gradient conditions, J. Geophys. Res., 112, 2007.

Thompson, G., Field, P. R., Rasmussen, R. M., and Hall, W. D.: Explicit Forecasts of Winter Precipitation Using an Improved Bulk Microphysics Scheme. Part II: Implementation of a New Snow Parameterization, Mon. Weather Rev., 136, 5095–5115, 2008.

Vetter, R., Sigg, S., Singer, H. M., Kadau, D., Herrmann, H. J., and Schneebeli, M.: Simulating isothermal aging of snow, Europhys. Lett., 89, 26 001, 2010.

Vionnet, V., Brun, E., Morin, S., Boone, a., Faroux, S., Le Moigne, P., Martin, E., and Willemet, J.-M.: The detailed snowpack scheme Crocus and its implementation in SURFEX v7.2, Geosci. Model Develop., 5, 773–791, 2012.

Wiesmann, A., Mätzler, C., and Weise, T.: Radiometric and structural measurements of snow samples, Radio Science, 33, 273–289, 1998.

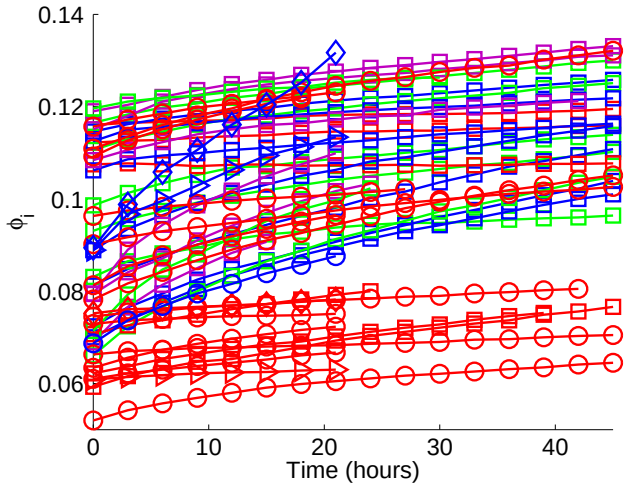

Fig. 1. Evolution of the ice volume fraction ϕ_i for all samples. Colors indicate different stress values: red 0 Pa, blue 133 Pa, green 215 Pa, magenta 318 Pa. Symbols indicated different temperatures: □ -18°C, ◯ -13°C, ▷ -8°C, ◊ -3°C)

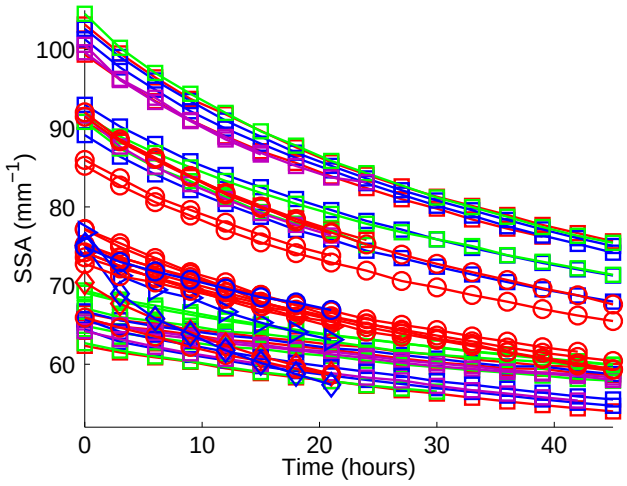

Fig. 2. Evolution of the SSA for all samples. Colors indicate different stress values: red 0 Pa, blue 133 Pa, green 215 Pa, magenta 318 Pa. Symbols indicated different temperatures: □ -18°C, ◯ -13°C, ▷ -8°C, ◊ -3°C)

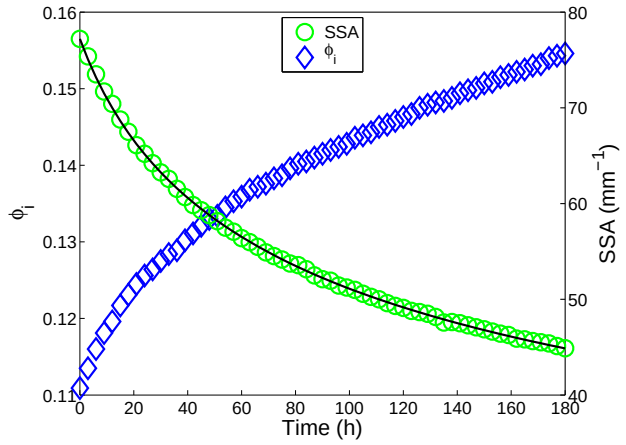

Fig. 3. Evolution of ice volume fraction and SSA in one week at about -13°C. The initial 3D structure and crystal habit of this experiment are shown in Figure 8 (bottom) and listed as snow 5 in Table 1. A fit of the SSA to Eq. (1) is plotted as black line.

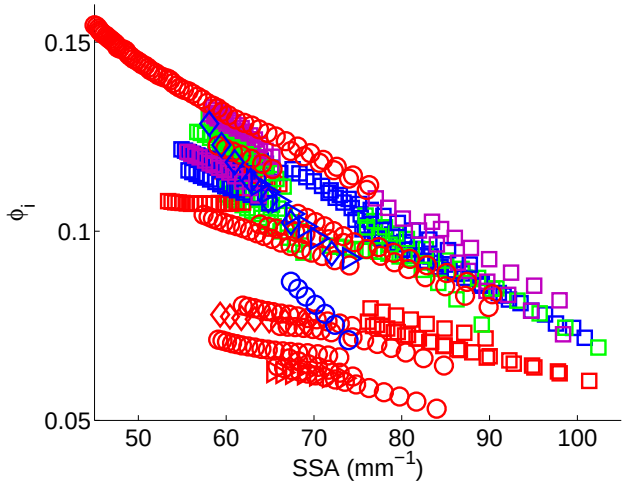

Fig. 4. Plot of the ice volume fraction versus the SSA for all experiments reveals an almost linear relation for each time series. Legend: stress indicated by colors: red 0 Pa, blue 133 Pa, green 215 Pa, magenta 318 Pa; temperature indicated by symbols: □ -18°C, ◯ -13°C, ▷ -8°C, ◊ -3°C;

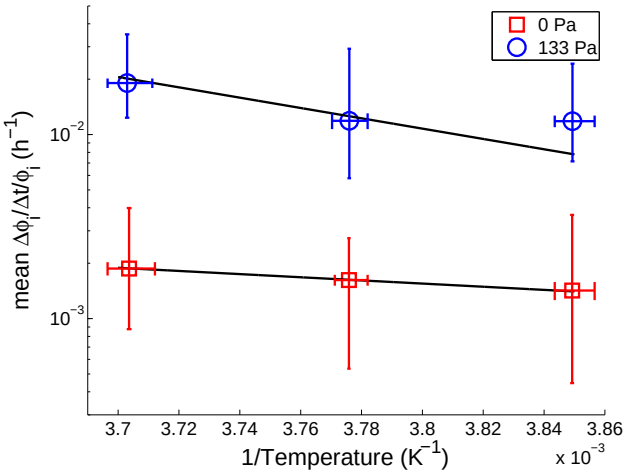

Fig. 5. Densification rate averaged over 24h as a function of temperature.

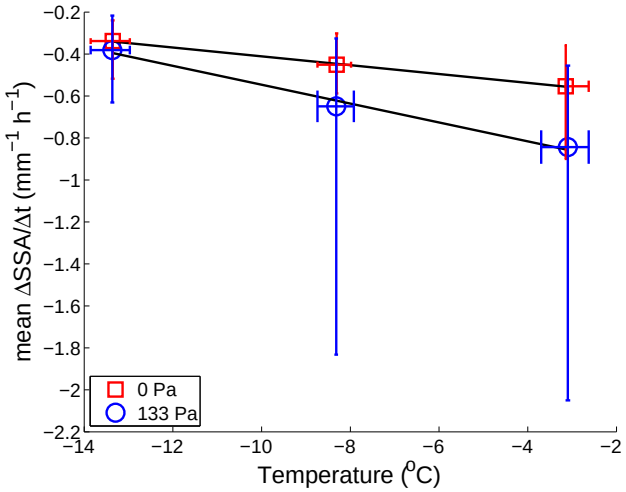

Fig. 6. SSA decay rate averaged over 24h as a function of temperature.

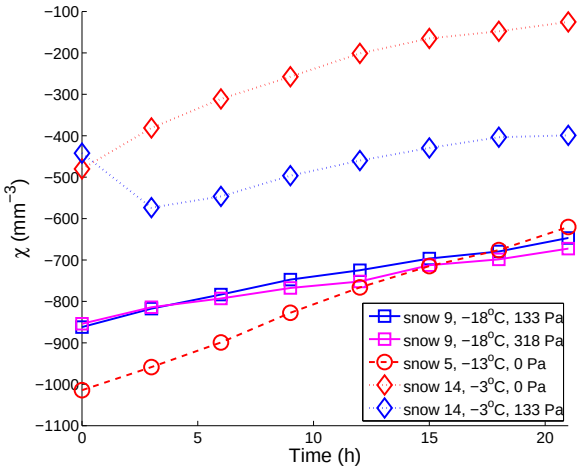

Fig. 7. Selected examples of the evolution of the Euler characteristic χ for different new snow types (cf. Table 1) during the first day of settlement: The one-week measurement (snow 5, Fig. 3), two examples of snow 9 with different applied stresses (taken from Schleef and Löwe (2013)), and two examples of snow 14 with different, applied stresses at -3°C.

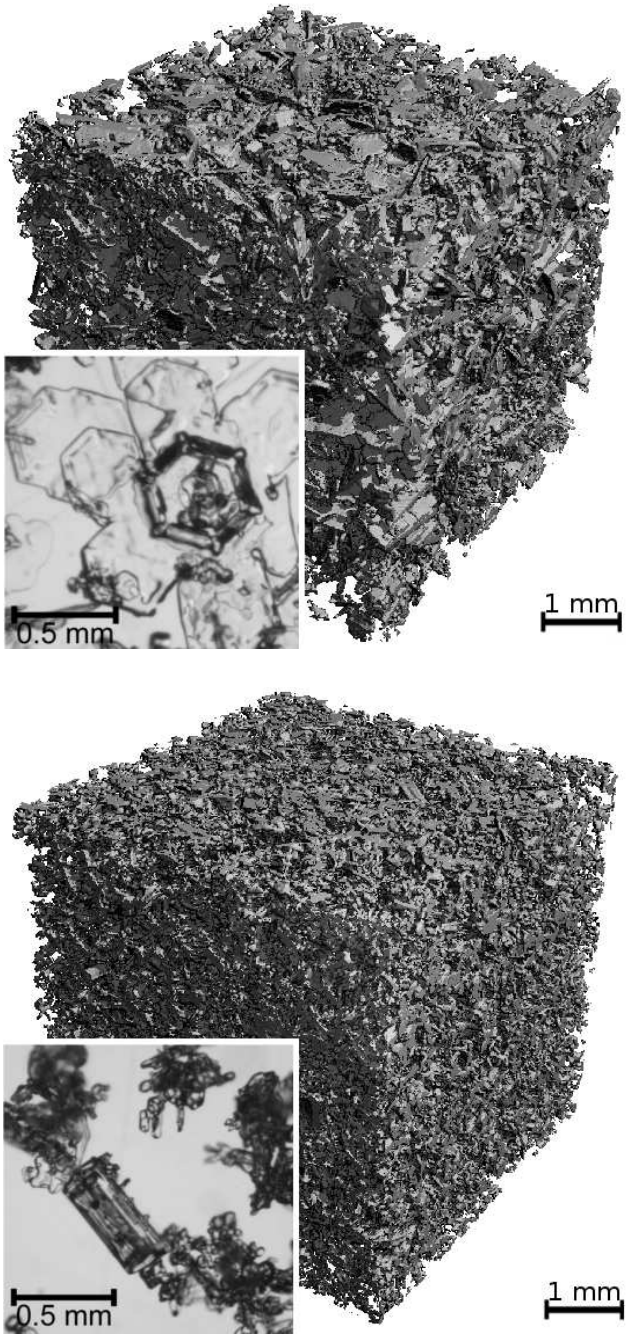

Fig. 8. Examples of natural snow samples with a photograph of the crystal habit and an μCT image of the initial structure. The parameters of the sample at top are $\phi_{\mathrm{i},0} \approx 0.1$ and $\mathrm{SSA}_0 \approx 62\mathrm{mm}^{-1}$ (snow 2 in Table 1), and of the sample at bottom $\phi_{\mathrm{i},0} \approx 0.1$ and $\mathrm{SSA}_0 \approx 77\mathrm{mm}^{-1}$ (snow 5 in Table 1, evolution shown in Fig. 3).

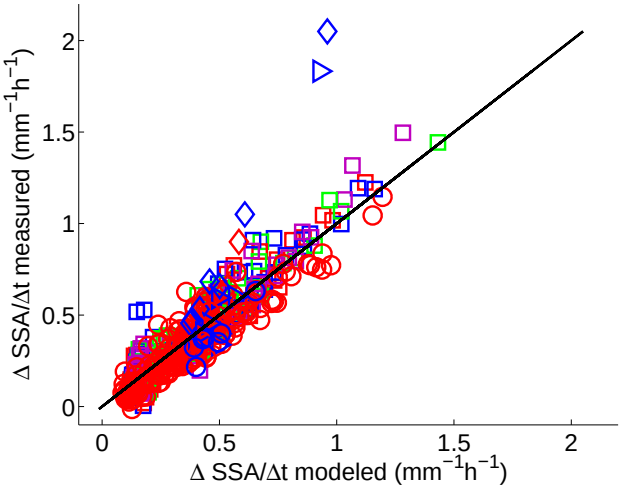

Fig. 9. Scatter plot of SSA decay rates $\dot{\mathrm{SSA}}$, computed from Eq. (4) (horizontal axis) versus measurements. Different stresses are indicated by colors: red 0 Pa, blue 133 Pa, green 215 Pa, magenta 318 Pa; different temperatures are indicated by the symbols: □ -18°C, ◯ -13°C, ▷ -8°C, ♢ -3°C; snow types are indistinguishable.

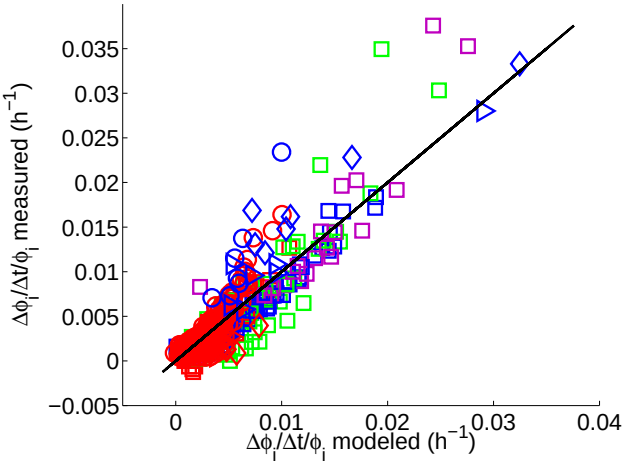

Fig. 10. Scatter plot of densification rates $\dot{\phi}/\phi$, computed from Eq. (7) (horizontal axis) versus measurements (vertical axis). Different stresses are indicated by colors: red 0 Pa, blue 133 Pa, green 215 Pa, magenta 318 Pa; different temperatures are indicated by symbols: □ -18°C, ◯ -13°C, ▷ -8°C, ♢ -3°C; snow types are indistinguishable.

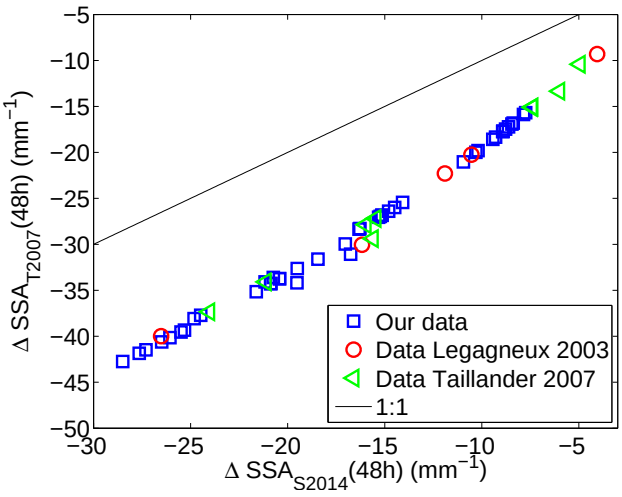

Fig. 11. Scatter plot of the predicted SSA difference $\Delta\mathrm{SSA}(48\mathrm{h})$ after 48h, obtained from the parametrizations Eq. (13) in Taillandier et al. (2007) (vertical axis) and from the present parametrization, Eq. (5) (horizontal axis), which were respectively applied to the different available datasets (legend).

Table 1. Overview of experiments. Set IDs (1-8) correspond to natural snow while (9-14) are snowmaker snow grown in the lab. The sets 9 and 10 were already used in Schleef and Löwe (2013) and included here for comparison. For each set the number of samples N_s and the total number of measurements N_m per sample in a time series are given in addition to applied stresses σ and used temperatures T. The initial values of ice fraction $\overline{\phi}_{\mathrm{i},0}$ and specific surface area $\overline{\mathrm{SSA}_0}$ are averages over all samples within the set. For all observed crystal habits the classification number is given according to Kikuchi et al. (2013), including potentially broken parts (I3a) of them.

Snow ID	N_s	N_m	σ Pa	T °C	$\overline{\phi}_{\mathrm{ice},0}$	$\overline{\mathrm{SSA}_0}$ mm^{-1}	Class. No.
1	2	32	133, 215	-18	0.08	92	P3a, P3b, R1c, H1a, I2a
2	5	76	0, 133, 215, 318	-18	0.11	64	P2b, P4c, P4d
3	7	90	0, 133, 215, 318	-18	0.07	102	P3a, R1c, I2a
4	4	43	0, 133, 215, 318	-18	0.08	91	P3b, R1c
5	2	68	0	-13	0.11	77	C3b, C3c, C4d, P3a, P3b, A1a
6	2	30	0	-13	0.09	75	P3b, P4e, P4f, A2a, R1c
7	2	24	0	-13	0.08	92	C4b, C4d, P2b, H1a, H1b
8	2	24	0	-13	0.06	86	P1a, P2a, P3a, P3b, P4e, P4g
9	7	111	0, 133, 215, 318	-18	0.11	66	not analyzed
10	2	32	215	-18	0.10	69	not analyzed
11	1	19	0	-13	0.07	74	P3b, P3c, P4c
12	2	23	0	-13	0.07	75	P3b, P3c
13	1	8	0	-13	0.12	66	C1a, C1b, C1c, I1a
14	6	48	0, 133	-3, -8, -13	0.08	74	P3b, P3c